Morphology of axisymmetric vesicles with encapsulated filaments and impurities

Akiyoshi SHIBUYA, Yukio SAITO and Hiroyuki HYUGA†
Department of Physics, Keio University, Yokohama 223-8522

(Dated: July 17, 2000)

The shape deformation of a three-dimensional axisymmetric vesicle with encapsulated filaments or impurities is analyzed by integrating a dissipation dynamics. This method can incorporate systematically the constraint of a fixed surface area and/or a fixed volume. The filament encapsulated in a vesicle is assumed to take a form of a rod or a ring so as to imitate cytoskeletons. In both cases, results of the shape transition of the vesicle are summarized in phase diagrams in the phase space of the vesicular volume and a rod length or a ring radius.

We also study the dynamics of a vesicle with impurities coupled to the membrane curvature. The phase separation and the associated shape deformation in the early stage of the dynamical evolution can well be explained by the linear stability analysis. Long runs of simulation demonstrate the nonlinear coarsening of the wavy deformation of the vesicle in the late stage.

I. INTRODUCTION

Amphiphilic molecules in the aqueous solvent assemble into a bilayer membrane, and form a closed vesicle. A typical example is an artificial lipid-bilayer, which serves as a model for biomembranes. Vesicles of a lipid-bilayer membrane have been studied as a model system of living cells over a couple of decades. In particular, after Helfrich proposed an elastic continuum model of the membrane [1], many works have been made about the morphology of the vesicles. Even in the case of a single component, vesicles take various shapes, and their shapes are classified as spherical, prolate, oblate, pear, stomatcyte and so on, according to Seifert et al.[2]

Actually, biomembranes might be more complex by containing many components such as several different species of lipids or membrane proteins. Impurity lipid molecules and proteins can move freely within the two-dimensional liquid state of the membrane and perform diffusive motion. Via the coupling to the membrane curvature, impurities may affect the shape of the vesicle. Also the vesicle can enclose cytoskeletons in its interior space. Cytoskeletons consist of microtubles and/or intermediate filaments, and form a three-dimensional network inside a cell to support the cell shape. Also for the cell locomotion, the elongation and the shortening of filamental proteins in the vesicle are required.[3] Thus in the study of living cells, the consideration of the interaction between lipid bilayer membranes and such encapsulated materials is indispensable.

To study the role of such materials, several experiments have been made. Hotani and Miyamoto[4] established a model system where microtubules polymerize in a vesicle. A growing microtuble pushes the vesicle membrane at contact points and deforms it into the shape resembling a Greek letter ϕ. There have been many experiments and theoretical analyses on this phenomenon. It was established that to realize the ϕ-shape, the osmotic pressure inside the vesicle has to be higher than the outer pressure,[5, 6] or the volume of the vesicle has to be fixed. [7, 8] It is also found that the monopolar asymmetric ϕ-shape has a lower energy and is stabler than the bipolar mirror symmetric shape.

When the filaments in the vesicle are soft such as actin filaments, they bend and form a ring in the vesicle. The experiment of such cases was performed by Miyata and Hotani[9]. They observed that ring filaments in a vesicle push the vesicle outward and deform the spherical vesicle into a disk shape.

Shape transformation caused by the phase separation within the membrane occurs in many important natural phenomena such as cell locomotion, fusion, secretion, endocytosis, phagocytosis etc. Furthermore, various experiments have been performed on this type of shape changes in multi-component vesicles. One example of the experiments is on the transition from a biconcave shape of erythrocytes to a crenated one (echinocytosis) [10, 11]. Another one is on a shape deformation induced by the phase separation of the amphiphiles composing the membrane[12]. Also there is an experiment on a shape deformation caused by proteins[13] or polymers which are anchored in membranes[14]. In these cases, vesicles transform from the spherical shape to the one with a budding or from a tubular shape to a pearling one. The effect of impurity on the vesicle morphology was first analyzed by S. Leibler[15]. He showed that the impurities diffusing within the two-dimensional membrane couple

†ashibuya@phys.keio.ac.jp; yukio@rk.phys.keio.ac.jp; hyuga@rk.phys.keio.ac.jp

to the curvature and destabilize the flat membrane. Recently, dynamical simulations of two-component vesicles have been performed [16] and the coalescence process of the budding vesicle was obverved[17].

In this paper, we study morphology of a three-dimensional axisymmetric vesicle with encapsulated filaments or embedded impurities, by solving purely dissipative dynamics. In section II, the model Hamiltonian of a vesicle is introduced, and its dissipative dynamics is formulated. In section III, the shape of the vesicle encapsulating a rod filament is studied. As a linear filament elongates, vesicular shape alters from a sphere to a rugby-ball, and to a sphere with tubular protrusions. The shape transition is summarized in a phase diagram in the phase space of the vesicular volume and a filament length. In section IV, we study the case of ring filaments. When filaments in the vesicle are soft such as actin filaments, they bend and form a ring. As the filament extends their length, the ring pushes out the vesicle membrane and deforms the prolate vesicle into the oblate one. In the case of cell division, the ring filament shrinks. Relations between the ring-force and the vesicle shape or the ring radius are studied in this case, and the morphological transition is summarized in the phase diagram. In section V, we study the effect of impurities embedded in the membrane on the vesicle shape, and observed that impurities diffusing within the vesicle surface induce curvature instability. A linear stability analysis around a spherical vesicle is confirmed in our simulation of the vesicle under several conditions. We have further simulated the nonlinear coalescing process in the late stage. Whole analysis is summarized in section VI.

II. DISSIPATION DYNAMICS OF MEMBRANES

The shape of a membrane vesicle is characterized by two parameters $s_i,\ (i=1,2)$ such that the position vector $\vec{r}$ of the membrane surface in three dimensional space is represented as $\vec{r}(s_1,s_2)$. With this parametrization, the metric tensor is given by $g_{ij}=\partial_i\vec{r}\cdot\partial_j\vec{r}$, and its determinant is denoted as $g=det\{g_{ij}\}$. Here ∂_i denotes the partial differentiation by s_i as $\partial_i=\partial/\partial s_i$. The surface area element is given by $dA=\sqrt{g}d^2s$ and the volume element by $dV=dA(\vec{r}\cdot\vec{n})/3$ where $\vec{n}$ is the surface normal vector.

The energy of the system consists of the bending elastic energy, and the surface and the volume contributions as

$$E=\frac{\kappa}{2}\int(H-C_0)^2dA+\sigma A+PV. \tag{1}$$

Here κ is the bending rigidity, H the mean curvature defined as the sum of two principal curvatures C_1 and C_2 as $H=C_1+C_2$, C_0 the spontaneous curvature, σ the surface tension, and P the pressure. In a dissipative dynamics, the system evolves to reach minimum energy configuration dictated by the energy (1). To achieve this purpose, we assume a purely dissipative dynamics with the Rayleigh dissipation function of the form

$$F_d=\frac{\eta}{2}\int|\vec{v}|^2dA. \tag{2}$$

with a viscosity coefficient η. The equation for time evolution is then written as [18, 19, 20]

$$\frac{\delta F_d}{\delta\vec{v}}=-\frac{\delta E}{\delta\vec{r}}. \tag{3}$$

This gives, in general, the shape evolution equation as

$$\partial_t\vec{r}=-\frac{1}{\eta\sqrt{g}}\frac{\delta E}{\delta\vec{r}}=v_n\vec{n}=(v_c-\eta^{-1}\sigma H-\eta^{-1}P)\vec{n}, \tag{4}$$

where the normal component of the velocity due to the curvature elasticity is given by

$$\eta v_c=\frac{\kappa}{2}\{H(C_1-C_2)^2+2\tilde{\Delta}H+4C_1C_2C_0\}. \tag{5}$$

Here $\tilde{\Delta}=g^{-1/2}\partial_i(g^{1/2}\partial^i)$ is the Beltrami-Laplace operator. This evolution equation (4) is explicitly derived by Marsili et al.[18] in section III.A.1-3 in their paper. Shape evolution generally induces variations of the surface area or the volume enclosed by the vesicle as[18, 19, 20]

$$\frac{dA}{dt}=\int H(v_c-\eta^{-1}\sigma H-\eta^{-1}P)dA, \tag{6}$$

$$\frac{dV}{dt}=\int(v_c-\eta^{-1}\sigma H-\eta^{-1}P)dA. \tag{7}$$

If the area of the vesicle is to be fixed, the tension σ should be regarded as a Lagrange multiplier, and has to be adjusted so as to satisfy $dA/dt=0$. If the volume as well as the surface area are to be fixed, both the tension σ and the pressure P have to be adjusted to yield: $dA/dt=dV/dt=0$.

For an axi-symmetric vesicle, the position vector is conveniently written in the cylindrical coordinate as (ρ,φ,z), where the z axis is chosen to be the axis of rotational symmetry. As for the two parameters, we choose an arclength $s_1=s=\int\sqrt{(dz)^2+(d\rho)^2}$ and the angle $s_2=\varphi$. The arclength is measured from the bottom of the vesicle on the symmetry z axis. The rotational symmetry tells us that the shape is independent of the second parameter $s_2=\varphi$. Then the metric is $\sqrt{g}=\rho$, the angle-integrated area element is $dA=2\pi\rho ds$ and the volume element is $dV=\pi\rho^2z_sds$. Since the shape is independent of the rotation angle φ, we consider hereafter a section at $\varphi=0$, and the vesicle contour is given in (ρ,z)-space. The normal and tangential vectors in this space are given as

$$\vec{n}=(z_s,-\rho_s),\quad \vec{t}=(\rho_s,z_s), \tag{8}$$

and two principal curvatures are calculated to be

$$C_1=z_s/\rho,\quad C_2=\rho_sz_{ss}-z_s\rho_{ss}. \tag{9}$$

Here the subscript s denotes differentiation by s, for instance, $z_s = \partial_s z$. The Beltrami-Laplace operator is represented as

$$\tilde{\Delta} = \frac{1}{\rho}\partial_s \left(\rho \partial_s\right). \tag{10}$$

The variation of the elastic energy produces only the normal component of the velocity, because only this component has the physical significance. Nevertheless, we introduce a tangential component of the velocity, which corresponds to the rearrangement of the parametrization s, or a *gauge*, on a vesicle surface. In the practice of shape simulation, we deal with only a discrete set of points (called grid points, hereafter) on the membrane. Even if these grid points are initially prepared in equidistance, they will dilatate or contract locally during the shape evolution. In order to redistribute grid points in equal separation, we must add an appropriate tangential velocity $v_t(s)\vec{t}$ at a grid point of an arclength s. Since the total arclength L varies in time, the condition of equal separation of grid points are expressed by imposing the invariance of a relative arclength, namely $d(s/L)/dt = 0$. By this condition, we get the tangential velocity[19, 20]

$$v_t(s) = -\int_0^s v_n C_2 ds + \frac{s}{L}\int_0^L v_n C_2 ds. \tag{11}$$

The evolution of a vesicle is then obtained by numerically integrating the equation

$$\frac{\partial \vec{r}}{\partial t} = v_n \vec{n} + v_t \vec{t}. \tag{12}$$

III. ENCAPSULATION OF ROD FILAMENT

We consider here vesicle deformation induced by the elongation of an encapsulated filaments such as microtubles. The filaments are rigid and extend straight in the vesicle. They push and deform the incarcerating vesicle. There have been several studies on this problem so far. [5, 6] We first reproduce known results by the present method. Since the encapsulated filament is assumed to remain straight, it exerts pressing force at both end points or poles at $s = 0$ and $s = L$ as $F\delta_0(s)$ and $F\delta_0(s - L)$, respectively. Here the invariant form of the delta function in the parameter space is given [18] as

$$\delta_0(\vec{s} - \vec{s}') = \frac{\delta(\vec{s} - \vec{s}')}{\sqrt{g}}. \tag{13}$$

In the equilibrium case, the forces balance equation around the pole is given by $\eta v_n(s) + F\delta_0(s) = 0$. By integrating over a very small area around the pole $s = 0$ with a radius ρ, the second term gives simply F, whereas in the first term only the Beltrami-Laplace term gives rise to nonvanishing contribution as

$$\kappa \int \rho^{-1}\partial_s(\rho\partial_s H) 2\pi\rho ds \approx 2\pi\kappa\rho\partial_\rho H. \tag{14}$$

Here we use the approximation such that around the pole at $s = 0$, the profile is almost horizontal and $ds = d\rho$. The integration of the force balance equation then yields the curvature [5] as

$$H(\rho) = H_0 - \frac{F}{2\pi\kappa}\log \rho/\rho_0, \tag{15}$$

where H_0 and ρ_0 are appropriate constants. This expression implies that the curvature diverges at the end $s = 0$ ($\rho = 0$) and the same type of divergence appears at the other end ($s = L$). Even though this diverging curvature, gives rise to only finite contribution to the bending energy, the vesicle shape at the poles cannot be derived by the dynamics governed by the curvature alone. To overcome this difficulty, both poles are pushed outwardly until the pole-separation ℓ reaches the prescribed length of the rod filament. When the pole-separation exceeds the prescribed distance ℓ, the poles are set free from external force and the distance decreases due to the curvature force by the nearby surface. The force applied on the poles are estimated from Eq.(15) by the curvature differences between ρ_1 and ρ_2 close to the poles as

$$F = 2\pi\kappa \frac{H(\rho_2) - H(\rho_1)}{\log \rho_1/\rho_2}. \tag{16}$$

Simulation results are normalized in the dimensionless form. The length is measured in unit of R_0, which is the radius of the sphere with a surface area of the vesicle, and the energy by $8\pi\kappa$. Then the volume is normalized by $4\pi R_0^3/3$, the pressure P as $p = PR_0^3/\kappa$ and the force F as $f = FR_0/4\pi\kappa$, respectively. In the simultaion the spontaneous curvature C_0 is set to be 0.

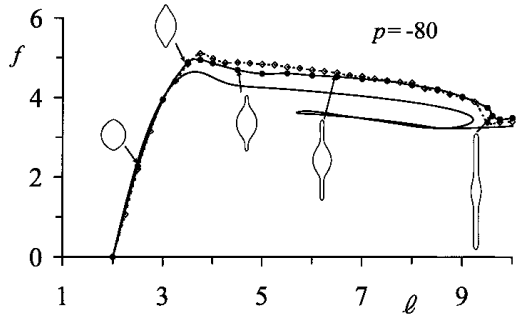

FIG. 1: Separation distance between two poles ℓ versus the strength of the force f for a vesicle under a pressure $p = -80$. Data obtained in the present analysis are depicted by the symbol •. A solid curve represents data obtained by the variational method by Umeda *et al.* [5]. Results obtained by the Monte Carlo simulation [6] are represented by the symbol ⋄.

We first summerize the results of the simulations with a fixed osmotic pressure p. By starting from the mirror-symmetric shape of the vesicle with symmetric forces at

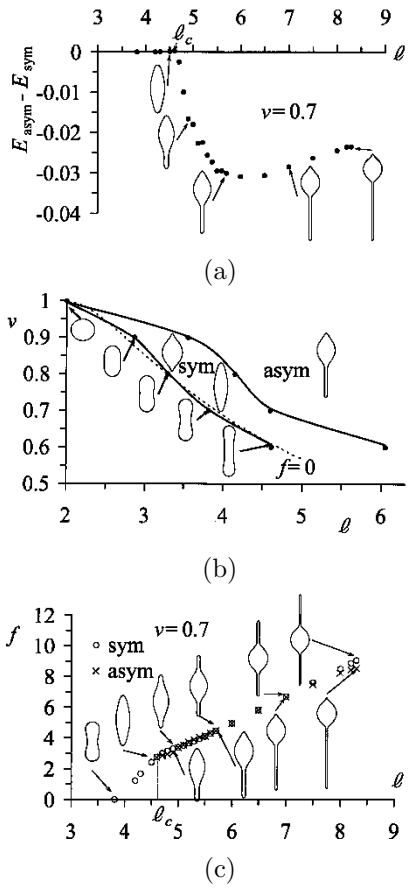

FIG. 2: (a) Energy difference of the assymmetric and the symmetric vesicle as a function of the rod length ℓ. The volume of the vesicle is fixed at $v = 0.7$. (b) Morphology phase diagram of the vesicles with various volume v and the rod length ℓ. A dashed curve indicates the cylinders with hemishperical caps at both ends. (c) The strength of the force f versus the rod length ℓ at a volume $v = 0.7$. The critical length for protrusion is $\ell_c = 4.6$.

both poles, we get the vesicle with a mirror symmetry about the equator. The shapes as well as the length-force relation are shown in Fig.1, in good agreement with those obtained previously. [5, 6] With a negative osmotic pressure, the elongation of the filament length ℓ inside a spherical vesicle leads first to the increase of the strength of the force f applied to both poles, but eventually f reaches the maximum when two poles start to protrude. The maximum value of f turns out to be a little larger than the value obtained by Umeda *et al.*, probably due to the relatively small number of grid points ($N = 120$) in our simulation. By applying asymmetric forces at both poles in the initial stage of the simulation, we can get an asymmetric shape. This is due to the fact that the asymmetric shape has a lower energy and is stabler than the mirror symmetric one, as is already discussed previously. [5, 6]

One of the advantage of the present method is that the shape of a vesicle with a fixed volume can be studied easily and quickly.[8] When the length of the rod is short, the vesicle takes a mirror symmetric shape independent of the initial condition. On the other hand when the rod is long and two protrusions appear, two distinct shapes, that is symmetric and asymmetric shapes, become possible. Both shapes have similar energies, but the energy difference between these two shapes at a volume $v = 0.7$ shown in Fig.2(a) indicates that the asymmetric shape is energetically favorable than the symmetric one. The morphological phase diagram is summarized in the phase space of the volume v and the rod length ℓ in Fig.2(b). Some typical shapes are shown therein. The phase boundary marked by $f = 0$ represents the $v - \ell$ relation for the free prolate shape without any force at poles. In order to decrease the volume under the condition of a fixed surface area, the vesicle changes its shape from sphere to prolate. In fact, the $v - \ell$ relation can be well explained by assuming that the vesicle takes the shape of a cylinder with hemispherical caps at both ends. The radius of the sphere r and the length of the cylinder $\ell - 2r$ should be determined from the conditions of constant surface area $4\pi r^2 + 2\pi r(\ell - 2r) = 4\pi$ and the constant volume $4\pi r^3/3 + \pi r^2(\ell - 2r) = 4\pi v/3$. The $v - \ell$ relation so determined is denoted by a dashed curve in Fig.2(b). For a cylinder part, one of the curvature vanishes, $C_2 = 0$. In the actual situation the vesicle lowers its elastic energy by selecting an appropriate value of C_2, and thus the phase boundary $f = 0$ deviates a little from the curve expected for the simplified cylindrical shape.

When the force is applied on two poles of the vesicle with a fixed volume, the rod length ℓ increases. For instance at $v = 0.7$, the strength of the force f increases as ℓ as shown in Fig.2(c). Initially, as the filament elongates, f increases rapidly until the poles begins to push out. Once one or both poles start to protrude, the increment of f gets mild. As the rod gets long, the tubular protrusion becomes thin with a small diameter, and the central bulb gets more rounded.

The shape of the vesicle under a strong force might be approximated by the form of a cylindrical tube attached to a spherical bulb. In order to fulfil the volume conservation, the sphere covers the volume $4\pi v/3$ such that its radius is just $v^{1/3}$. Since the sphere gives only the area $4\pi v^{2/3}$, the remaining area is covered by the fine cylindrical tube with an extension ℓ' and the radius $r \approx 2(1-v^{2/3})/\ell'$. For $\ell' \to \infty$, the volume of the cylinder vanishes $\pi r^2 \ell' \sim 1/\ell' \to 0$. Therefore, the rhs region of the phase diagram in Fig.2(b) extends to infinity except at $v = 1$.

IV. ENCAPSULATION OF RING FILAMENT

When the filaments encapsulated are soft like actin filaments, they tend to bend and to form a ring in a

vesicle. As their degree of polymerization or their length increases, the ring radius expands. On the contrary, in the case of cell division, an actin filament ring shrinks.

The force exerted by the ring at $z = 0$ can be estimated by assuming the force balance: $\eta v_n(z = 0)+F/2\pi r\delta(z) = 0$. Here F is the strength of the total force exerted by the ring of radius r at $z = 0$. Similar to Eq.(14), an area integration around $z = 0$ can be performed with $\rho \approx r$ and $ds = dz$. Then it yields the curvature as

$$H(z) = H_0 - \frac{F}{2\pi\kappa r}z. \tag{17}$$

where H_0 is the curvature at $z = 0$. In this case, H_0 remains finite. The total force applied by the ring at $z = 0$ is estimated from Eq.(17) by taking the curvature difference as

$$F = 2\pi r\kappa\frac{H_0 - H(z_1)}{z_1}. \tag{18}$$

We now simulate the shape variation of the vesicle induced by the force exerted by the ring filaments. Every physical quantity is scaled in the dimensionless form as before. For a given volume $v = 0.7$, the free vesicle has a prolate shape with a radius about $r \approx 0.42$ at the equator $z = 0$, and the other curvature C_2 is negative. As the ring radius increases, the bending energy increases, as shown in Fig.3(a). Correspondingly, the force calculated by the formula Eq.(18) also increases, as shown in Fig.3(b). The dotted curve shows the result obtained by numerically differentiating the energy shown in Fig.3(a) by the radius r. This indirect calculation of the force agrees well with the force obtained directly from the simulation until the force passes the maximum for the prolate shape and the minimum for the oblate shape.

With a small increment of the radius, the curvature C_2 at the equator is still negative. On increasing the ring radius, the central zone expands to have two positive curvatures, still keeping the two poles far apart as in the prolate shape. As the central radius increases, the force to expand the radius starts to weaken. At a large enough radius as $r > 1.14$, the prolate becomes unstable and the vesicle jumps to an oblate shape. The oblate at $r = 1.23$ is, in fact, a shape with a local minimum energy without a force. It has a bending energy being a little more than that of the prolate shape, and thus is a metastable shape. On the further increase of the ring radius, the shape changes to that of a flying saucer with a large energy cost. On decreasing the ring radius from that of the free oblate shape, the dips at poles deepen. At a small ring radius, another dips develope at the equator, too. Actually, the bending energies of the prolate and the oblate shapes cross at a critical radius $r_c = 0.96$ for the fixed volume $v = 0.7$, and the first-order shape transition should take place there. The morphology phase diagram with prolate and oblate shapes is shown in the phase space of the volume v and the ring radius r as shown in Fig.3(c).

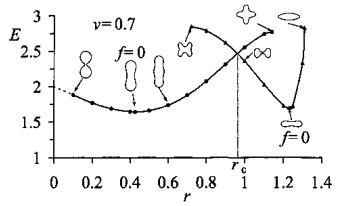

(a)

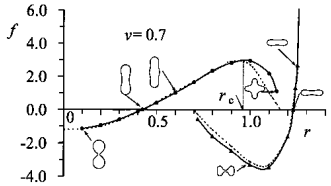

(b)

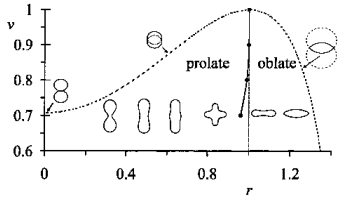

(c)

FIG. 3: (a) Bending energy E versus ring radius r of a vesicle with a volume $v = 0.7$ for the prolate (filled circles) and the oblate (filled triangles) shapes. Lines are guides for the eyes. (b) The strength of the radial force f versus the radius r at the equator. A dashed lines indicate the strength of the force induced by the derivative of the bending energy. (c) Morphological phase diagram in v and r space. A dashed curve indicateds the upper and lower limiting shapes (see text). The critical radius is $r_c = 0.96$.

When the ring shrinks in the middle of the prolate shape from the natural radius $r = 0.42$, as in the case of cell division, the two parts, the northern and the southern area, get round, as shown in Fig.3(a) and (b). Since the surface area and the volume of the vesicle are fixed, the central radius can vanish only for a vesicle with a normalized volume less than $1/\sqrt{2} \approx 0.71$. When the volume is larger than this value, the shrinkage stops intermediately with a shape of two connected hemispheres.

When the volume is smaller than this value, the shape of the vesicle at $r = 0$ is equivalent to the two connected equilibrium shapes with half of the volume. As shown in Fig.3(a), when the volume of the vesicle is 0.7, the vesicle approaches to the shape with two connected almost spherical shapes with $v = 0.99$, where the bending energy of the vesicle is about 2.

When the ring shrinks or expands in a vesicle with a fixed volume and a fixed surface area, there is a certain

limit for the ring radius r determined solely by the geometric reason. For a ring with a minimum radius r, the vesicle takes the symmetrical semi-spherical shape; the radii of upper and lower spheres are the same as R and the separation between two centers is $2d$. For a ring with a maximum radius r, the vesicle again takes the symmetric semi-spherical shape with the separation between two centers equal $2d$ being negative. The area conservation gives the condition $4\pi R(R+d) = 4\pi$, and the volume conservation $2\pi(R+d)^2(2R-d)/3 = 4\pi v/3$. The radius at the equator is given by $r = \sqrt{2-R^{-2}}$. When $d = R = 1/\sqrt{2}$, the vesicle consists of two complete spheres with $r = 0$ and the volume is equal $v = 1/\sqrt{2}$. When $d = -R = -\infty$, the vesicle becomes flat with a vanishing volume $v = 0$, but the radius at the equator remains finite $r = \sqrt{2}$. The upper and lower limits of r for arbitrary volume v can be easily obtained numerically, and are shown by a dashed curve in Fig.3(c). At $v = 0.7$, the upper limit of the radius r thus obtained agrees well with the result of dynamical simulation.

V. IMPURITY DIFFUSION

There are usually various ions or proteins dispersed in a membrane, and they affect the shape of vesicles. When the impurities are homogeneously distributed, the vesicle takes a shape determined by the curvature elasticity with some modification in the spontaneous curvature. But when the impurities are coupled to the local curvature of the membrane, the homogeneous distribution may become unstable. The phase separation and the shape instability are induced simultaneously. We here study this phenomenon analytically and numerically.

A Dynamics driven by impurities

Since the homogeneously distributed impurities only modify the spontaneous curvature and the surface tension σ, we set the average concentration to be zero. The local concentration fluctuation of intercalated molecules from the average 0 is denoted by $\Phi(\vec{r},t)$. The interaction of intercalated molecules with the phospholipidic constituents of the membrane might be summarized in the form,

$$F_{int} = -\Lambda \int d^D s\sqrt{g} H\Phi. \tag{19}$$

with a coupling constant Λ. The free energy of the impurity molecules is assumed to be Landau-Ginzburg form as

$$F_{imp} = \int d^D s\sqrt{g}[\frac{1}{2}B(\vec{\nabla}\Phi)^2 + f(\Phi)], \tag{20}$$

where the homogeneous part is expanded up to the fourth order as

$$f(\Phi) = \frac{A_2}{2}\Phi^2 + \frac{A_4}{4}\Phi^4. \tag{21}$$

Since the average fluctuation of impurity concentration is set to zero, there is no linear term of Φ in the free energy $f(\Phi)$. The evolution dynamics of the membrane, Eq.(3) now contains terms due to the impurity as

$$v_n = v_c + \eta^{-1}\Lambda\{2C_1C_2\Phi - \tilde{\Delta}\Phi\} - \eta^{-1}\{\tfrac{B}{2}(\partial_s\Phi)^2(C_1-C_2) + (\tfrac{A_2}{2}\Phi^2 + \tfrac{A_4}{4}\Phi^4)H\} - \eta^{-1}\sigma H - \eta^{-1}P. \tag{22}$$

The conservation of the total number of impurity molecules on the membrane leads to the restriction $\int d^D s\sqrt{g}\Phi = 0$. Therefore, the time-evolution of the impurity concentration fluctuation Φ should satisfy

$$0 = \frac{d}{dt}\int d^D s\sqrt{g}\Phi = \int d^D s\sqrt{g}(\frac{\partial\Phi}{\partial t} + \Phi H v_n). \tag{23}$$

This is satisfied by describing the evolution in terms of the diffusion equation as

$$\partial_t\Phi + \Phi H v_n = D\tilde{\Delta}\left(\frac{1}{\sqrt{g}}\frac{\delta F}{\delta\Phi}\right). \tag{24}$$

In a simulation where a membrane is discretized into grid points, the supporting grid points have a tangential velocity in addition to the physical normal velocity, so as to keep the grid separation equidistant. Accordingly, the concentration fluctuation field Φ should include this contribution given as

$$\delta\Phi = \frac{\partial\Phi(\vec{r}(t))}{\partial t}\,\delta t = \frac{\partial\vec{r}}{\partial t}\cdot\nabla\Phi\;\delta t = v_t\partial_s\Phi\;\delta t. \tag{25}$$

Therefore, the final evolution for Φ is described as

$$\partial_t\Phi + \Phi H v_n - v_t\partial_s\Phi = D\tilde{\Delta}(-B\tilde{\Delta}\Phi + A_2\Phi + A_4\Phi^3 - \Lambda H). \tag{26}$$

We introduce the following dimensionless parameters hereafter.

$$\phi = \Phi R_0^2, \quad b = \frac{B}{\kappa R_0^4}, \quad a_2 = \frac{A_2}{\kappa R_0^2}, \quad a_4 = \frac{A_4}{\kappa R_0^6}, \quad \lambda = \frac{\Lambda}{\kappa R_0}, \quad d = \eta D R_0^4, \quad c_0 = C_0 R_0. \tag{27}$$

B Linear stability analysis

In this section we study the stability of the spherical vesicle with homogeneously distributed impurities under a small shape fluctuation and the impurity inhomogeneity. For simplicity, we consider the case with a fixed pressure P, and thus the volume of the vesicle can be altered. In the unperturbed situation, the vesicle has a radius R_0. Assuming the small deformation of the vesicle and no overhang configuration, the vesicular position

vector $\vec{r}$ and the concentration of impurities ϕ in dimensionless form are single-valued functions of the polar θ and the azimuthal angle φ in the spherical coordinate. These small deviations are expanded in terms of spherical harmonic function Y_m^l, and we note that each mode is independent in the linear stability analysis. Therefore, one considers only the l-pole mode, and the membrane position vector $\vec{r}$ and the impurity concentration ϕ in dimensionless form are written as

$$\vec{r}(\theta,\varphi,t) = \{1+\delta_m^l(t)Y_m^l(\theta,\varphi)\}\vec{e}_r(\theta,\varphi), \qquad (28)$$

$$\phi(\theta,\varphi,t) \qquad = \zeta_m^l(t)Y_m^l(\theta,\varphi). \qquad (29)$$

where δ and ζ describe the time-dependent coefficients of fluctuations and $\vec{e}_r$ is the unit radial vector. Since the average concentration is set to zero, there is no unperturbed term in the expansion of the concentration ϕ. From Eqs.(22) and (26), one obtains the linear dynamics of the perturbation δ_m^l, ζ_m^l as

$$\frac{\partial\delta_m^l}{\partial t} \simeq (l+2)(l-1)\left\{-l(l+1)+\frac{1}{2}p+c_0\right\}\delta_m^l + \{2\lambda+\lambda l(l+1)\}\,\zeta_m^l, \qquad (30)$$

$$\frac{\partial\zeta_m^l}{\partial t} \simeq d\left\{-l(l+1)\left[bl(l+1)+a_2\right]\zeta_m^l + \lambda l(l+1)(l+2)(l-1)\delta_m^l\right\}. \qquad (31)$$

The conservation of the surface area determines the surface tension σ. With a small shape deformation δ, the variation of σ is easily shown to be quadratic in δ, and it does not affect the linear stability analysis. Eqs. (30) and (31) can be reduced to matrix from as follows.

$$\begin{pmatrix} \partial_t\delta_m^l \\ \partial_t\zeta_m^l \end{pmatrix} = \begin{pmatrix} -(l+2)(l-1)\left\{l(l+1)-\frac{p}{2}-c_0\right\} & \{2+l(l+1)\}\lambda \\ dl(l+1)(l+2)(l-1)\lambda & -dl(l+1)\{bl(l+1)+a_2\} \end{pmatrix}\begin{pmatrix} \delta_m^l \\ \zeta_m^l \end{pmatrix}$$
$$\equiv \begin{pmatrix} M_{rr} & M_{r\phi} \\ M_{\phi r} & M_{\phi\phi} \end{pmatrix}\begin{pmatrix} \delta_m^l \\ \zeta_m^l \end{pmatrix}. \qquad (32)$$

Note that the time-development matrix M is independent of m. The eigenvalues β_+, β_- and eigenvectors $(\delta_\pm, \zeta_\pm)$ of the matrix M define the time evolution of the deviations δ_m^l, ζ_m^l as follows.

$$\begin{pmatrix} \delta_m^l \\ \zeta_m^l \end{pmatrix} \quad = A_+\exp(\beta_+ t)\begin{pmatrix} \delta_+ \\ \zeta_+ \end{pmatrix} + A_-\exp(\beta_- t)\begin{pmatrix} \delta_- \\ \zeta_- \end{pmatrix}, \qquad (33)$$
$$\beta_\pm = \tfrac{1}{2}\{M_{rr}+M_{\phi\phi} \pm \sqrt{(M_{rr}-M_{\phi\phi})^2+4M_{r\phi}M_{\phi r}}\},$$
$$\begin{pmatrix} \delta_\pm \\ \zeta_\pm \end{pmatrix} = \begin{pmatrix} M_{r\phi} \\ -M_{rr}+\beta_\pm \end{pmatrix}.$$

In Fig.4 we show the relationship between the growth rate β_+, β_- and mode number l for both cases without $\Lambda = 0$ (solid curves) and with the coupling $\Lambda \neq 0$ (dashed curves).

With a negative a_2, as in Fig.4(b) impurities can phase separate spontaneously, i.e. even if there is no coupling to the curvature of the membrane, $M_{\phi\phi} > 0$ for $l^* \geq 1$ when $2b < -a_2$. Then the most unstable mode $l^*_{\Lambda=0}$ is the integer close to $1/2(-1+\sqrt{1-2a_2/b})$. When $2b < -a_2 \leq 6b$, the most unstable mode is $l^* = 1$. The impurities tend to phase separate into two domains. With a small coupling to the membrane curvature ($\Lambda \neq 0$), this mode induces the translation of the vesicle without deformation. When $6b < -a_2$, some modes with $l^* \geq 2$ becomes unstable. With a small coupling Λ, the vesicle deforms accordingly.

To confirm the linear stability analysis and further to elucidate the nonlinear effect, we simulate the dynamical evolution of the vesicular shape and the impurity diffusion. We assume axisymmetry in the simulation, and thus only $m = 0$ modes are relevant here. The parameters chosen are $b = 0.1,\ a_2 = -1,\ a_4 = 1,\ \lambda = 3.0,\ d = 1,\ c_0 = 0$. The pressure p is fixed to be $p = 0$. The most unstable mode is expected to be $l^* = 6$.

The initial shape is spherical, and the impurities are distributed randomly whose Fourier amplitudes up to 32nd mode ζ_0^ℓ for $\ell \leq 32$ have uniformly distributed between -0.001 and 0.001. In the course of simulation the vesicle shape developes the wavy pattern with 6 domains of impurities, as shown in Fig.5(a). Impurities accumulate to the convex portion of the vesicle due to the positive coupling $\Lambda > 0$. This number corresponds to the most unstable mode with $l^* = 6$. As the time evolves, these domains coalesce each other. In last stage of Fig.5(c) the number of the domains becomes 4.

With a positive a_2, accumulation of impurities costs energy and they try to diffuse away to be homogeneous if there is no coupling to the curvature of the membrane. However, due to the coupling between the concentration variation and the membrane curvature, the homogeneous distribution can be unstable and the phase separation is possible for sufficiently strong coupling as shown in Fig.4(a). The linear stability analysis shows that a spherical vesicle becomes unstable if the coupling is stronger

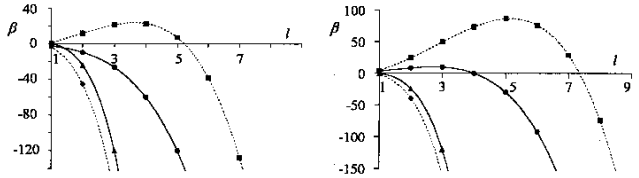

(a) (b)

FIG. 4: Growth rate β as a function of mode number l in the linear stability analysis for P=0, $C_0 = 0$, (a) for $a_2 > 0$, (b) for $a_2 < 0$. Solid curves represent the growth rates for $\Lambda = 0$, β_+ (filled circles) and β_- (filled triangles). Dashed curves represent the growth rates for $\Lambda \neq 0$, β_+ (filled squares) and β_- (filled diamonds). The parameters are $b = 0.1,\ a_2 = 1$ or $-2,\ a_4 = 1,\ \lambda = 2.0\ d = 1,\ c_0 = 0, p = 0$.

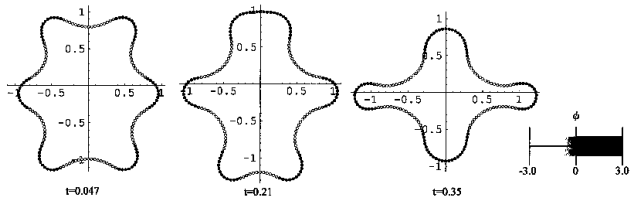

(a) (b) (c)

FIG. 5: Time evolution of the vesicle with impurities, the parameters are $b = 0.1,\ a_2 = -1,\ a_4 = 1,\ \lambda = 3.0\ d = 1,\ c_0 = 0, p = 0$. The most unstable mode is $l^* = 6$ The time is measured in unit of $\eta R_0^4/\kappa$.

than the critical value $|\lambda^*| = \sqrt{18b + 3a_2}/2$. For the parameter choice $b = 0.1,\ a_2 = 1,\ a_4 = 1,\ d = 1,\ c_0 = 0$, the critical coupling takes the value $\lambda^* \sim 1.09$. When the coupling is stronger than λ^* such as $\lambda = 3.0$, the most unstable mode has $l^* = 6$, in good agreement to the early stage of the simulation result as shown in Fig.6(a).

By decreasing the coupling such as $\lambda = 2.5$, the number of the most unstable mode decreases to $l^* = 5$, in agreement to the simulation result shown in Fig.7(a). When the correlation length b gets smaller such as $b = 0.05$, the number of the most unstable mode increases as $l^* = 9$. In the simulation the vesicle becomes wavy with 8 domains in the early stage as shown in Fig.8(a). The result has the same tendency with the linear stability analysis. In all the cases studied, the coarsening takes place as the time elapses, and the number of domains decreases.

We can study the effects of the pressure p or the spontaneous curvature c_0 by linear analysis. According to Eq.(32), the positive p or c_0 increase the number of the most unstable mode l^*. On the contrary the negative p or c_0 decrease l^*. For example, we simulated

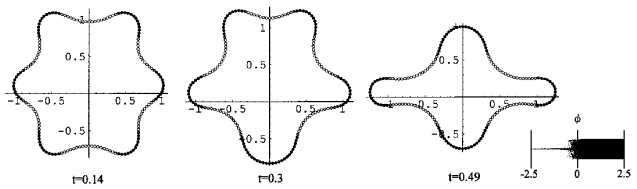

(a) (b) (c)

FIG. 6: Time evolution of the vesicle with impurities, the parameters are $b = 0.1,\ a_2 = 1,\ a_4 = 1,\ \lambda = 3.0\ d = 1,\ c_0 = 0, p = 0$. The most unstable mode is $l^* = 6$

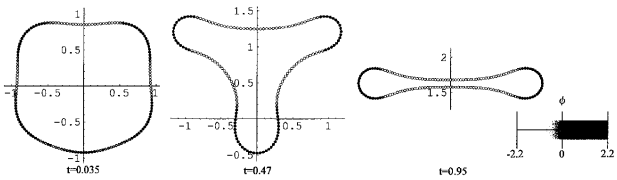

(a) (b) (c)

FIG. 7: Time evolution of the vesicle with impurities, the parameters are $b = 0.1,\ a_2 = 1,\ a_4 = 1,\ \lambda = 2.5\ d = 1,\ c_0 = 0, p = 0$. The most unstable mode is $l^* = 5$

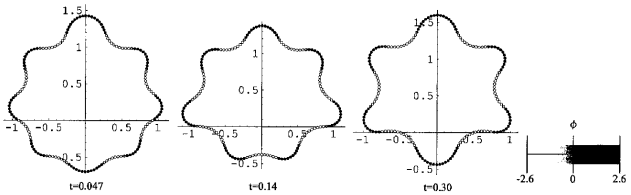

(a) (b) (c)

FIG. 8: Time evolution of the vesicle with impurities, the parameters are $b = 0.05,\ a_2 = 1,\ a_4 = 1,\ \lambda = 3.0\ d = 1,\ c_0 = 0, p = 0$. The most unstable mode is $l^* = 9$

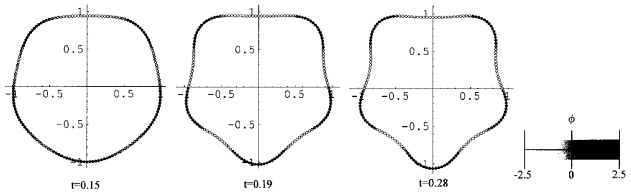

(a) (b) (c)

FIG. 9: Time evolution of the vesicle with impurities, the parameters are $b = 0.1,\ a_2 = 1,\ a_4 = 1,\ \lambda = 3.0\ d = 1,\ c_0 = 0, p = -40$. The most unstable mode is $l^* = 5$

the shape of the vesicle with the parameters such as $p = -40,\ b = 0.1,\ a_2 = 1,\ a_4 = 1,\ \lambda = 3.0\ d = 1,\ c_0 = 0$ as shown in Fig.9. Then the linear analysis gives the most unstable mode $l^* = 5$, in fair agreement with the simulation. From Fig.9(b) and (c), the coarsening does not seem to take place under the pressure. This might be related to the resistence to the volume change at a negative p.

In almost all cases the results of the simulation in the early stage agree with the linear stability analysis. Moreover, the phase separation domains coalesce each other, as the time evolves. This nonlinear coalescing process is also observed in the previous study[17].

VI. CONCLUSION

We performed simulations of the axisymmetric vesicle shape change caused by the length change of an encapsulated ring or rod filaments. The constant volume simulation of the vesicle with a rod encapsulation shows that the ϕ shape consisting of a spherical and a tubular portions is attributed to the restriction of the volume and the surface area conservations. The same restriction limits the extention of the ring radius in the case of the ring-filament encapsulation. The shape transitions of the vesicle are summarized in phase diagrams, Fig.2(b) and 3(c), in the phase space of the vesicular volume and a rod-filament length or a ring-filament radius. [5, 6, 7, 8].

We also performed simulations on the dynamics of the vesicle shape caused by the phase separation of the impurity concentration. Impurities which show spontaneous phase separation induces periodic deformation in the vesicle shape. Even those impurities which do not give rise to spontaneous phase separation are shown to induce periodic deformations through the strong coupling of the impurity concentration to the membrane curvature. The early stage is well explained by the linear stability analysis, such as the dominant periodicity of the shape deformation. In late stage where the nonlinear effect becomes dominant, the coarsening of the shape periodicity takes place. Similar coasening process was observed in the previous study[17]. The study on the strongly deformed vesicle due to the impurity phase separation is now under way.

REFERENCES

[1] W. Helfrich: Z. Naturforsch. C**28**, (1973) 693.
[2] U. Seifert, K. Berndl, and R. Lipowsky: Phys. Rev. A**44**, (1991) 1182.
[3] D. Bray: *Cell Movements* (Garland Publishing, New York, 1992).
[4] H. Hotani, and H. Miyamoto: Adv. Biophys. **26**, (1990) 135.
[5] T. Umeda, H. Nakajima, and H. Hotani: J. Phys. Soc. Jpn. **67**, (1998) 682.
[6] R. Morikawa, Y. Saito, and H. Hyuga: J. Phys. Soc. Jpn. **68**, (1999) 1760.
[7] D. K. Fygenson, J. F. Marko, and A. Libehaber: Phys. Rev. Lett. **79**, (1997) 4497.
[8] V. Heinrich, B. Bozic, S. Svetina and B. Zeks: Biophys. J. **76**, (1999) 2056.
[9] H. Miyata, and H. Hotani: Proc. Natl. Acad. Sci. USA **89**, (1992) 11547.
[10] B. Deuticke: Biochem. Biophys. Acta. **163** , (1968) 494.
[11] D. Allan, and R. H. Michell: Nature **258**, (1975) 348.
[12] C. Gebhardt, H. Gruler, and E. Sackmann: Z. Naturforsch. **32c**, (1977) 581.
[13] A. J. Bradley, E. Maurer-Spurej, D. E. Brooks, and D. V. Devine: Biochemistry **38**, (1999) 8112.
[14] I. Tsafrir, D. Sagi, T. Arzi, M-A. G-Boudeville, V. Frette, D. Kandel, and J. Stavans: Phys. Rev. Lett. **86**, (2001) 1138.
[15] S. Leibler: J. Physique **47**, (1986) 507.
[16] T. Taniguchi: Phys. Rev. Lett. **76**, (1996) 4444.
[17] P.B. S. Kumar, G. Gompper, R. Lipowsky: Phys. Rev. Lett. **86**, (2001) 3911.
[18] M. Marsili, A. Maritan, F. Toigo, and J. R. Banavar: Rev. Mod. Phys. **68**, (1996) 963.
[19] S. Langer, R. Goldstein and D.P. Jackson: Phys. Rev. A**46**, (1992) 4894.
[20] I. Cantat, C. Misbah, and Y. Saito: Eur. Phys. J. E**3**, (2000) 403.